1.10 Instrumental Background

In this section, we present an analysis of measurements performed during the flat-field tests at XRCF to determine the instrumental background rates and rejection efficiencies of the ACIS flight CCDs. The mean rates and spectral shapes of the instrumental background in the ACIS detectors are presented in Section 1.10.1. Results showing the dependence of background rejection efficiency on event grade selection are reported in Section 1.10.2. The measured background rates from the XRCF data are then used to estimate on-orbit background rates in Section 1.10.3.

1.10.1 Background Rate Measurements at XRCF

Instrumental background measurements at XRCF were performed between flat-field tests, while the energy of the X-ray source was being changed. The data were acquired with the ACIS door in the open position. During each background measurement, the small gate valve where the X-ray beam line enters the thermal vacuum chamber was closed. Occasionally, however, the gate valve was opened by the TRW test director to facilitate tuning of the X-ray source in preparation for the next flat-field test. The background measurements were acquired in 11 science runs performed during the period 1997 May 10–18. For each run, ACIS was operated in either imaging or spectroscopy array mode, with all six detectors in the appropriate array read out. The ACIS telemetry event lists used in this analysis are identified by Science Run Number and TRW ID in Table 1.69.

Science Run	TRW ID	ACIS Array
76	I-BND-BU-2.027	Imaging
85	I-BND-BU-2.025	Spectroscopy
90	I-BND-BU-2.003	Imaging
99	I-BND-BU-2.029	Spectroscopy
105	I-BND-BU-2.013	Imaging
109	I-BND-BU-2.015	Spectroscopy
113	I-IAI-BG-3.001	Imaging
127	I-IAS-BG-3.002	Spectroscopy
150	I-IAS-BG-3.902	Spectroscopy
152	I-IAI-BG-3.901	Imaging
155	I-IAI-BG-3.901A	Imaging

Table 1.69: XRCF Phase I Science Runs Used for the Instrumental Background Analysis

Frames were processed for events by the ACIS electronics using the standard event thresholds for front-illuminated (38 ADU) and back-illuminated (20 ADU) ACIS detectors, along with the standard split threshold of 13 ADU. The exposure time per frame was 3.34 s. Light curves were then plotted showing the number of counts per frame vs. frame number. Periods of time when the gate valve was open were easily identified by the abrupt increase in the number of counts per frame. The range of frame numbers contaminated by X-rays were noted and all events in these frames were removed from the event lists. The events in each list were then sorted into spectra by detector quadrant and event grade.

For each detector, we combined the spectra from all the science runs to increase the signal-to-noise. The total exposure time thus obtained was $\sim$ 63.9 ks for each imaging array detector, and $\sim$ 49.2 ks for each spectroscopy array detector. Detectors S2 and S3 are in both arrays and so had total exposures of $\sim$ 113.1 ks each. To further improve the statistics, we combined the spectra from all eight front-illuminated (FI) flight CCDs. Unfortunately, we could not do the same for the back-illuminated detectors. The ACIS focal plane operating temperature at XRCF was $-110\,^{\circ}$C; this is $10\,^{\circ}$C warmer than the designed operating temperature. Consequently, the background data taken at XRCF with detector S1 were contaminated by an increase in the number of hot pixels and could not be used in the instrumental background analysis.

Rejection of particle-induced events in the ACIS detectors is accomplished using event amplitude and event grade selection criteria (i.e., the sum and distribution of charge in 3×3-pixel events). The passband of the ACIS detectors folded with the HRMA is $\sim$ 0.1–10 keV, so we rejected all events with total pulse-height amplitudes greater than 10 keV. This eliminated 19.5% of the 781,015 events accumulated in the FI detectors and 80.0% of the 26,636 events accumulated in detector S3. We then applied the standard ASCA G02346 event grade selection criteria to the data to reject all events with pixel geometries that were inconsistent with the physical interaction of X-rays in the ACIS detectors (i.e., ASCA G157 events). The results are presented in Figures 1.103 & 1.104.

The upper panel of Figure 1.103 shows the spectrum from 0.1–10 keV of the background events that were rejected by the ASCA G02346 selection criteria in the FI detectors. The rejected background rises abruptly from zero at low energies to a peak of about 0.32 ct cm^{-2} s^{-1} keV at around 0.65 keV, then decays towards higher energies as a power law with index around -2.2, and finally levels off above 6 keV into a long, flat tail with amplitude ~ 1–2×10^{-3} ct cm^{-2} s^{-1} keV^{-1}. Spectrally-integrated background rates are listed in Table 1.71.

The lower panel of the figure shows the spectrum of the background events in the FI detectors that were not rejected by the event grading scheme. These unrejected background events masquerade as true X-ray events. The spectrum of the unrejected background appears essentially flat from 0.1–10 keV, with the exception of two emission lines. The

Mn Kα line at 5.894 keV is due to scattered X-rays from the internal contamination monitor (ICM), while the Au Lα line at 9.671 keV is caused by particle-induced fluorescence in the detector framestore covers.

The spectrum of the rejected background events in detector S3 is shown in the upper panel of Figure 1.104. The spectrum suffers from low counting statistics, but a small peak can be seen around 0.4 keV; the spectrum then drops between 1 keV and 4 keV, before rising with energy in a broad hump that peaks around 13 keV.

The lower panel shows that the unrejected background in S3 is also relatively flat, with the exception of the Au Lα line and a apparent excess in the number of counts below 2 keV. Note there is no sign of an Mn Kα line in the spectrum.

To study the spatial distribution of the Mn Kα line in the focal plane, we have measured the flux of the line in each quadrant. The Mn Kα line fluxes in each detector are listed in Table 1.70, along with the fluxes of the Au Lα line and the unrejected continuum background. The last column contains the mean and RMS deviation of the count rates in the quadrants. The Mn Kα rate varies systematically with position on the focal plane. All of the scattered Mn Kα flux is observed in detectors I0 and I1, and the quadrants of I2 and I3 immediately adjacent to I0 and I1, respectively. The collimator and baffling of the internal contamination monitor was intended to require at least two reflections for a photon to travel from the source itself to the focal plane. The diffuse reflectance of the gold-coated surfaces near the detectors is$\leq 2 \times 10^{-5}$ sr^{-1} at 6 keV. The (unbaffled) brightness of the ICM source itself was about 3×10^{3} ph sr^{-1} during the June 1997 XRCF measurements. Had the ICM baffling requirement been met, the observed flux at the focal plane (some 14 cm from the source) should have been less than 10^{-8} ph cm^{-2} s^{-1}. The observed rate on I0 and I1 suggests that a subtantial fraction of the source flux is arriving at the detectors after a single reflection. The reason for this is not understood. For reference, a diagram showing the ICM, the focal plane, and the intended ICM beam patterns is presented in Figure 1.105.

The total Mn K_α flux in I0 and I1 is about 3.2×10^{-4} ct cm^{-2} s^{-1}, while the estimated continuum flux under the peak (unrejected) is about 4.1×10^{-5} ct cm^{-2} s^{-1}. Thus, the scattered Mn K_α photons increased the instrumental background in the 5.9 ± 0.06 keV spectral band by a factor of ~ 8.6 at XRCF. Assuming AXAF is launched in January or February of 1999, about 20 months will have elapsed since the XRCF measurements were made. Given the 2.7 year half-life of the Fe 55 source in the ICM, the predicted on-orbit rate for the Mn K_α line drop by a factor of about 2/3. Moreover, since the expected amplitude of the on-orbit continuum exceeds that observed at XRCF by about a factor of about 50 (see Section 1.10.3 below), the scattered ICM is expected to increase the on-orbit background by about 10% in the 5.9 ± 0.06 keV band.

Returning to Table 1.70, we see that the Au Lα fluxes and the continuum fluxes are

Flight Device	Source	Quad A	Quad B	Quad C	Quad D	Mean (RMS)
		($\times$ 10^{-4} ct cm^{-2} s^{-1})				
I0	Mn K_α	2.59 ± 0.56	2.07 ± 0.51	2.07 ± 0.51	3.52 ± 0.63	2.56 ± 0.68
	Au L_α	0.93 ± 0.40	1.76 ± 0.49	1.14 ± 0.42	1.24 ± 0.43	1.27 ± 0.35
	Cont.	13.15 ± 1.48	11.50 ± 1.44	12.74 ± 1.44	10.87 ± 1.48	12.06 ± 1.06
I1	Mn K_α	4.04 ± 0.68	3.21 ± 0.62	4.04 ± 0.68	3.62 ± 0.65	3.73 ± 0.40
	Au L_α	1.14 ± 0.42	0.93 ± 0.40	0.93 ± 0.39	1.04 ± 0.40	1.01 ± 0.10
	Cont.	11.60 ± 1.54	14.19 ± 1.57	12.74 ± 1.56	12.63 ± 1.54	12.79 ± 1.06
I2	Mn K_α	3.31 ± 0.61	0.83 ± 0.36	0.00 ± 0.21	0.00 ± 0.21	1.04 ± 1.57
	Au L_α	1.04 ± 0.39	1.86 ± 0.51	1.86 ± 0.50	1.14 ± 0.43	1.48 ± 0.45
	Cont.	10.25 ± 1.43	13.25 ± 1.43	12.73 ± 1.34	13.36 ± 1.32	12.40 ± 1.46
I3	Mn K_α	0.00 ± 0.15	0.10 ± 0.21	1.35 ± 0.43	3.73 ± 0.66	1.29 ± 1.73
	Au L_α	0.73 ± 0.36	1.45 ± 0.44	1.24 ± 0.43	0.41 ± 0.33	0.96 ± 0.47
	Cont.	11.70 ± 1.20	9.43 ± 1.17	11.19 ± 1.34	13.15 ± 1.53	11.37 ± 1.54
S0	Mn K_α	0.00 ± 0.24	0.00 ± 0.19	0.00 ± 0.20	0.00 ± 0.14	0.00 ± 0.00
	Au L_α	0.81 ± 0.43	1.88 ± 0.56	1.88 ± 0.57	2.02 ± 0.59	1.65 ± 0.56
	Cont.	13.72 ± 1.48	9.55 ± 1.37	11.70 ± 1.48	11.97 ± 1.50	11.73 ± 1.71
S2	Mn K_α	0.00 ± 0.16	0.06 ± 0.17	0.23 ± 0.20	0.23 ± 0.20	0.13 ± 0.12
	Au L_α	0.64 ± 0.27	1.46 ± 0.34	0.99 ± 0.31	1.23 ± 0.33	1.08 ± 0.35
	Cont.	13.92 ± 0.98	12.64 ± 0.99	12.87 ± 0.98	12.81 ± 0.99	13.06 ± 0.58
S4	Mn K_α	0.00 ± 0.14	0.27 ± 0.30	0.00 ± 0.24	0.00 ± 0.27	0.07 ± 0.13
	Au L_α	1.35 ± 0.51	1.21 ± 0.49	1.48 ± 0.54	1.08 ± 0.51	1.28 ± 0.17
	Cont.	11.98 ± 1.44	12.92 ± 1.51	16.55 ± 1.67	17.09 ± 1.67	14.63 ± 2.56
S5	Mn K_α	0.40 ± 0.33	0.54 ± 0.36	0.13 ± 0.27	0.00 ± 0.24	0.27 ± 0.25
	Au L_α	1.61 ± 0.52	1.21 ± 0.49	1.08 ± 0.47	1.21 ± 0.49	1.28 ± 0.23
	Cont.	10.36 ± 1.43	11.97 ± 1.49	11.03 ± 1.39	12.51 ± 1.46	11.47 ± 0.96
S1*	Mn K_α	...	...	...	...	...
	Au L_α	...	...	...	...	...
	Cont.	...	...	...	...	...
S3	Mn K_α	0.23 ± 0.24	0.06 ± 0.23	0.00 ± 0.21	0.00 ± 0.20	0.07 ± 0.11
	Au L_α	0.53 ± 0.30	1.58 ± 0.40	0.82 ± 0.35	0.94 ± 0.34	0.97 ± 0.44
	Cont.	22.47 ± 1.23	24.93 ± 1.33	26.80 ± 1.33	22.41 ± 1.23	24.15 ± 2.12

* Background data taken at XRCF for detector S1 were contaminated by an increase in the number of hot pixels as a result of operating the focal plane at $-110°$ C.

Table 1.70: Instrumental Background Fluxes Measured at XRCF in the Passband 0.1–10 keV

roughly uniform across the focal plane, although a constant model is formally rejected in each case. The mean Au Lα line flux was $(1.25 \pm 0.069) \times 10^{-4}$ ct cm^{-2} s^{-1} in the FI detectors, and $(0.97 \pm 0.22) \times 10^{-4}$ ct cm^{-2} s^{-1} in S3. This ratio is consistent, within the rather large errors, with the expected relative quantum efficiency of the front- and back-illuminated detectors at 9.7 keV (see section 1.8.) Because the effective area of the ACIS/HRMA is so low at the energy of the Au Lα line, researchers observing faint diffuse sources can easily remove this extra source of background by applying a high-energy cutoff.

The mean background continuum fluxes for ASCA grade G02346 and G157 events are listed in Table 1.71. The errors quoted in the table are the standard deviations of the means. These measurements indicate that the total particle-induced count rate in a frontside device is about 26 times higher than the rate in a backside device, but the rejection efficiency of the frontside device is about 52 times better, so the net result is that the unrejected background rate in a backside device is about twice that of a frontside device.

Flight Device	Unrejected Events (G02346) (ct cm^{-2} s^{-1} keV^{-1})	Rejected Events (G157) (ct cm^{-2} s^{-1} keV^{-1})	Rejection Efficiency (%)
FI	$1.24 \pm 0.29 \times 10^{-4}$	$2.02 \pm 0.05 \times 10^{-2}$	99.4
S3	$2.42 \pm 0.11 \times 10^{-4}$	$5.26 \pm 0.23 \times 10^{-4}$	68.5

Table 1.71: Mean Background Continuum Fluxes Measured at XRCF in the Passband 0.1–10 keV

1.10.2 Dependence of Background Rejection Efficiency on Event Grade Selection

An important consideration in choosing ACIS event selection criteria is the efficiency of background rejection. To illustrate this point, we present in Tables 1.72, 1.73 and 1.74, the fraction of background events in various grades. For conciseness, we list only the standard ASCA grades, and ACIS grade 255. A similar analysis should be performed (presumably by the AXAF Science Center) for all 255 ACIS grades before a final decision is made on the definition of standard ACIS grades. Of course, the raw XRCF background event lists we have compiled are available to ASC for this purpose.

A cursory analysis of these tables shows, for example, that in device I3 91.21% of background events were ACIS bit map grade 255 events (i.e. all eight neighboring pixels were above the split threshold). However, only 4.14% of the background events in S3 were ACIS grade 255 events. Thus, a large majority of the background events in a frontside device could be rejected simply by filtering ACIS grade 255 events, but only a very small percentage of the background events in a backside device would be rejected. If one were to reject only ACIS grade 255 events, the total on-orbit background rate for six devices should be ~ 40 ct s^{-1}, which is about 22% of the telemetry bandwidth.

1.10.3 Predicted On-orbit Background Rates

To obtain predicted on-orbit instrumental background rates from the rates measured at XRCF, we scaled the XRCF count rates by the ratio of the on-orbit cosmic-ray flux to the cosmic-ray flux at the Earth's surface. As a first step, we analyzed simultaneous high-speed tap and telemetry data from sequence 1 of science runs 113 and 127 for detectors I3 (FI) and S3 (BI), respectively. To determine the cosmic-ray (CR) flux incident on each detector we plotted the ACIS events frame-by-frame, examined the distribution of events by eye, and decided how many cosmic rays were responsible for creating the events. Using this method the observed cosmic-ray flux, averaged over the upper hemisphere, was $(4.08 \pm 0.10) \times 10^{-3}$ CR cm^{-2} s^{-1} sr^{-1} in both I3 and S3.

According to Reinhold Müller-Mellin, principal investigator of the EPHIN instrument on AXAF, the cosmic-ray flux at the Earth's surface is fairly constant over a timescale of a day, with day-to-day variations of less than 1%. Interplanetary transients from solar events (called Forbush decreases) can cause decreases in the flux by 3–10%, while increases of a few percent are sometimes seen due to rare ground-level events. Long-term variations over the 11 year solar cycle result in variations of 15–20%. Thus, we can obtain a reasonably good check on our estimate of the cosmic-ray flux at XRCF by comparing it to the cosmic-ray flux measured by the EPHIN instrument during the AXAF thermal vacuum tests at TRW in 1998 June. Müller-Mellin analyzed 2 hours of EPHIN data on 1998 June 7 and found the cosmic-ray flux, averaged over the upper hemisphere, to be $(4.04 \pm 0.40) \times 10^{-3}$ CR cm^{-2} s^{-1} sr^{-1}. This is in excellent agreement with the value given above for the cosmic-ray flux measured at XRCF.

The cosmic-ray flux outside the influence of the Earth's magnetic field, (i.e. for eneriges exceeding 50 Mev/nucleon), is approximately 2 CR cm^{-2} s^{-1} [30]. Assuming this were the particle flux incident on the detectors, the predicted on-orbit background rates in ASCA grades 02346 would be $\sim 1.0 \times 10^{-2}$ ct cm^{-2} s^{-1} keV^{-1} in an ACIS frontside device, and $\sim 1.8 \times 10^{-2}$ ct cm^{-2} s^{-1} keV^{-1} in an ACIS backside device.

A second estimate of the AXAF background may be derived from measurements obtained with SOHO and reported by the EPHIN team. The so-called INT channel of EPHIN's sibling on SOHO measures a total flux of 0.38 ct cm^{-2} s^{-1} sr^{-1} in its orbit at L1. This channel integrates all electrons with energies in excess of 8 MeV and all nucleons with energies in excess of ~ 50 Mev/nucleon. If all of these particles interacted with the

ACIS as if they were minimum ionizing muons (the dominant cosmic-ray daughter species observed at sea-level), we would expect about twice the background listed above at the ACIS focal plane (i.e., about 2–4 $\times$ 10^{-2} ct cm^{-2} s^{-1} keV^{-1}). We have made no attempt to model the interaction of the actual on-orbit particle spectrum with the instrument. A significant fraction of the high energy protons observed in the INT channel will penetrate directly to the detectors (which are shielded with about 10 g cm^{-2} of Al). If we arbitrarily assume that energetic protons comprise all of the events detected in the INT channel, then the INT rate provides an upper limit to the expected on-orbit ACIS background. To the extent that some INT events are high energy ($E > 10$ MeV) electrons, this assumption is incorrect.

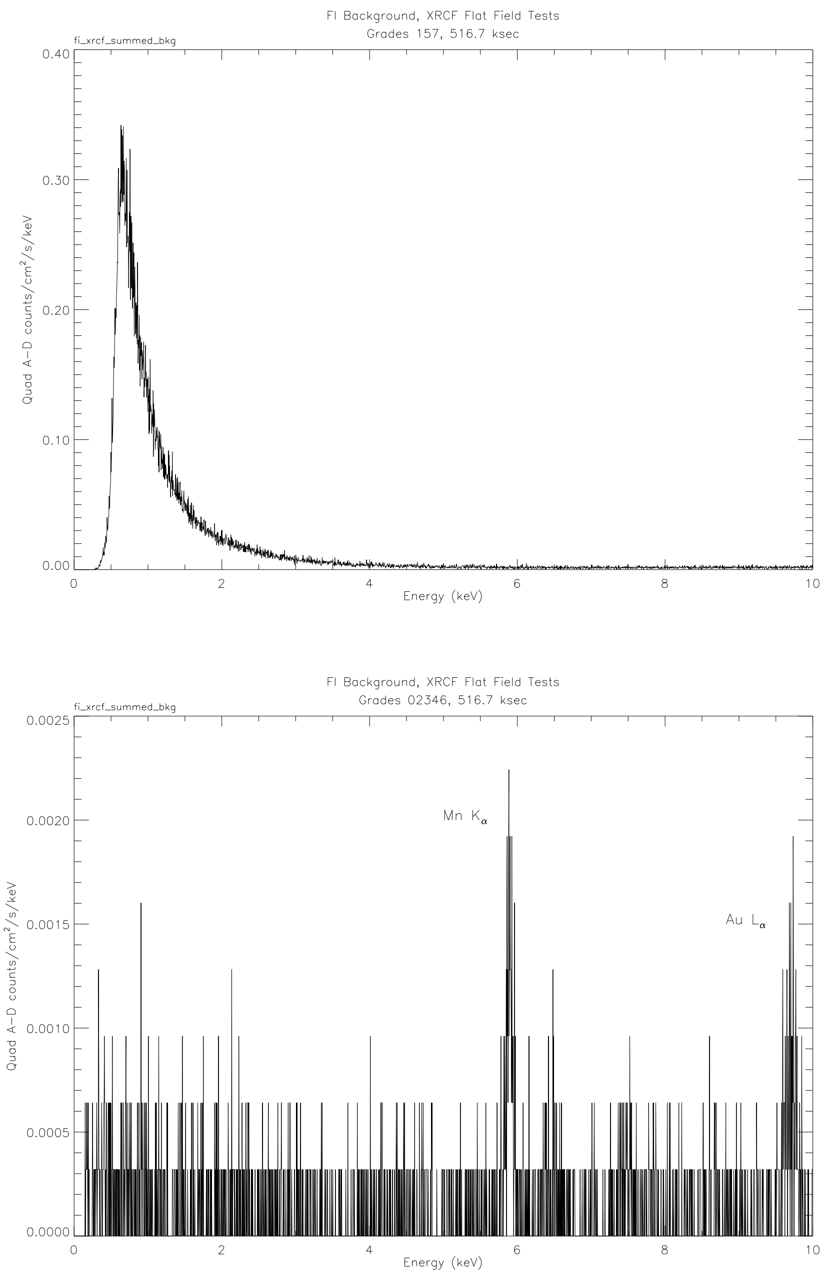

Figure 1.103: Background spectra measured at XRCF in the ACIS front-illuminated flight devices. The spectra have been summed over the four quadrants of all eight front-illuminated flight devices. The upper and lower panels show the spectra of the rejected (ASCA grades 157) and the unrejected (ASCA grades 02346) background events, respectively, in the passband 0.1–10 keV. The lower panel shows Mn K_α line emission due to scattered X-rays from the internal contamination monitor. The Au L_α line is caused by particle-induced fluorescence in the framestore covers.

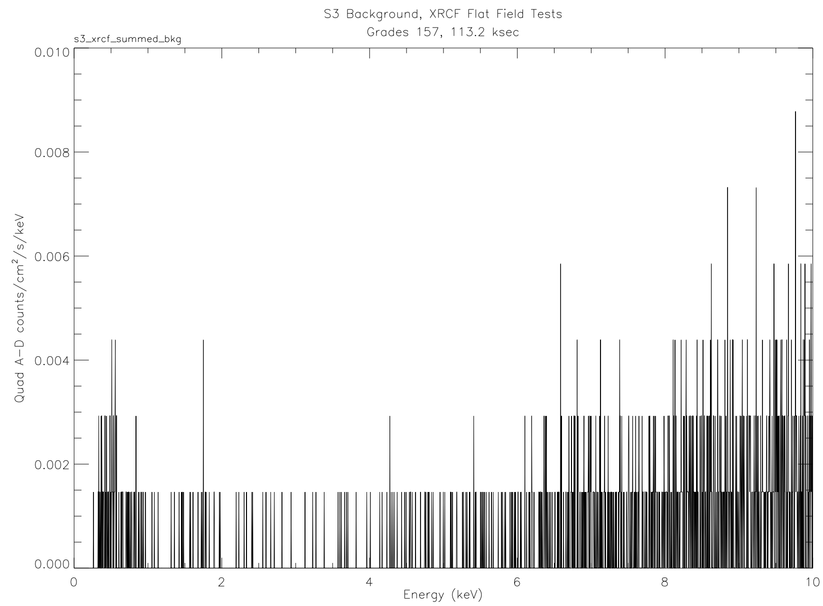

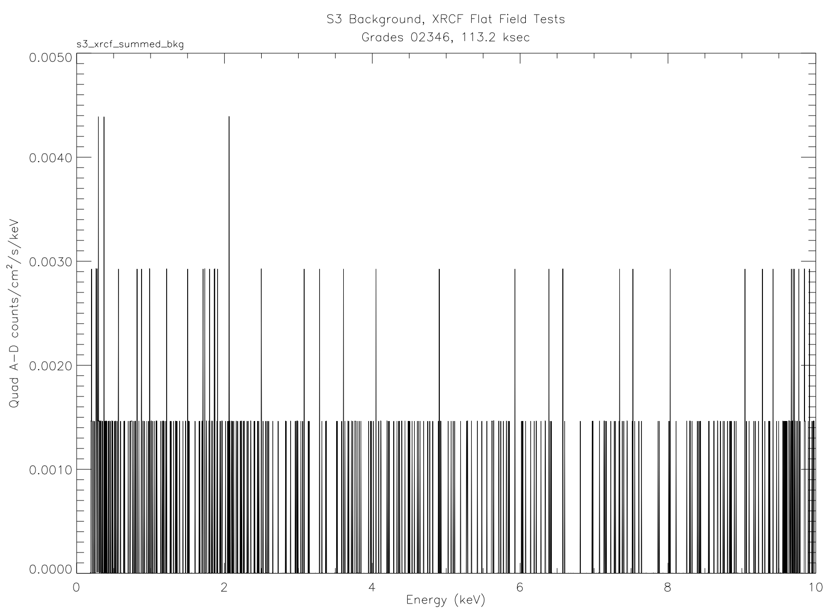

Figure 1.104: Background spectra measured at XRCF in the ACIS back-illuminated flight device S3. The spectra have been summed over all four quadrants. The upper and lower panels show the rejected (ASCA grades 157) and the unrejected (ASCA grades 02346) background spectra, respectively, in the passband 0.1–10 keV.

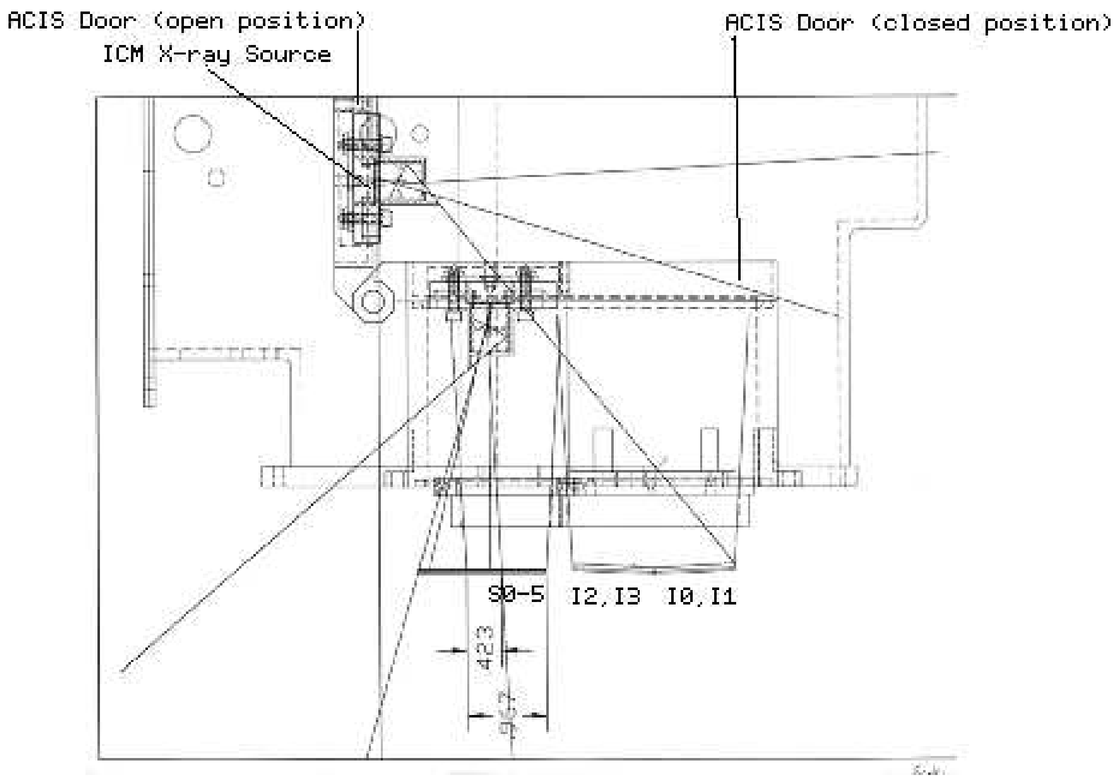

Figure 1.105: Cross-section through the ACIS detector housing showing the internal contamaination monitor (ICM) X-ray source, its intended illumination pattern, and the ACIS focal plane. In the drawing the Observatory X-axis is up and the Z axis points to the right. Scattered X-ray flux from the ICM is detected on chips I0 and I1, as well as on high-Z quadrants of chips I2 and I3. The scattering path is unknown. The two dimensions shown are in inches.

Flight Device	Event† Grades	Fraction of Events per Event Grade				
		Quad A	Quad B	Quad C	Quad D	Mean
		(%)				
I0	0	0.387	0.395	0.289	0.325	0.349
	1	0.000	0.000	0.000	0.000	0.000
	2	0.139	0.146	0.133	0.121	0.134
	3	0.050	0.052	0.066	0.047	0.054
	4	0.064	0.057	0.076	0.063	0.065
	5	0.144	0.130	0.152	0.173	0.150
	6	0.159	0.120	0.166	0.236	0.170
	7	99.059	99.101	99.118	99.036	99.078
	157	99.202	99.231	99.270	99.209	99.228
	B255	93.677	88.740	89.959	91.731	91.027
I1	0	0.354	0.423	0.355	0.354	0.371
	1	0.000	0.000	0.005	0.000	0.001
	2	0.204	0.146	0.143	0.106	0.150
	3	0.094	0.146	0.069	0.087	0.099
	4	0.077	0.065	0.103	0.087	0.083
	5	0.160	0.173	0.197	0.143	0.168
	6	0.166	0.179	0.172	0.133	0.163
	7	98.945	98.868	98.956	99.090	98.965
	157	99.105	99.041	99.158	99.232	99.134
	B255	91.637	89.269	90.800	91.361	90.767
I2	0	0.343	0.280	0.273	0.230	0.282
	1	0.000	0.004	0.000	0.004	0.002
	2	0.124	0.068	0.104	0.121	0.104
	3	0.057	0.055	0.056	0.042	0.053
	4	0.033	0.093	0.048	0.079	0.063
	5	0.129	0.140	0.164	0.155	0.147
	6	0.114	0.157	0.130	0.113	0.129
	7	99.199	99.202	99.226	99.256	99.221
	157	99.327	99.346	99.390	99.415	99.370
	B255	94.400	90.730	90.750	93.887	92.441
I3	0	0.247	0.197	0.346	0.327	0.279
	1	0.009	0.000	0.000	0.000	0.002
	2	0.085	0.081	0.059	0.163	0.097
	3	0.052	0.031	0.054	0.058	0.049
	4	0.019	0.063	0.069	0.062	0.053
	5	0.190	0.175	0.139	0.125	0.157
	6	0.166	0.103	0.129	0.192	0.148
	7	99.231	99.350	99.204	99.072	99.214
	157	99.430	99.524	99.342	99.197	99.373
	B255	90.273	90.925	90.304	91.679	90.795

† All event grades except B255 are ASCA grades. Here B255 stands for ACIS bit grade code 255 (i.e., all pixels above threshold).

Table 1.72: Fraction of Background Events per Event Grade Measured at XRCF in the Passband 0.1–10 keV for Detectors I0, I1, I2, and I3

Flight Device	Event† Grades	Fraction of Events per Event Grade (%)				
		Quad A	Quad B	Quad C	Quad D	Mean
S0	0	0.195	0.230	0.307	0.263	0.249
	1	0.000	0.000	0.000	0.006	0.001
	2	0.141	0.075	0.080	0.140	0.109
	3	0.060	0.027	0.043	0.053	0.045
	4	0.054	0.016	0.068	0.047	0.046
	5	0.124	0.166	0.141	0.169	0.150
	6	0.135	0.107	0.123	0.105	0.118
	7	99.291	99.379	99.239	99.218	99.282
	157	99.416	99.545	99.380	99.393	99.434
	B255	93.414	90.934	90.052	94.130	92.133
S2	0	0.393	0.298	0.338	0.354	0.346
	1	0.000	0.000	0.000	0.000	0.000
	2	0.179	0.158	0.143	0.156	0.159
	3	0.089	0.084	0.065	0.049	0.072
	4	0.066	0.056	0.068	0.052	0.061
	5	0.241	0.152	0.182	0.192	0.192
	6	0.241	0.155	0.169	0.182	0.187
	7	98.790	99.096	99.034	99.015	98.984
	157	99.031	99.248	99.216	99.207	99.176
	B255	90.966	88.295	88.005	90.258	89.381
S4	0	0.345	0.323	0.411	0.393	0.368
	1	0.000	0.000	0.007	0.008	0.004
	2	0.161	0.232	0.166	0.283	0.210
	3	0.112	0.074	0.151	0.039	0.094
	4	0.032	0.066	0.094	0.063	0.064
	5	0.209	0.182	0.216	0.157	0.191
	6	0.145	0.190	0.144	0.283	0.190
	7	98.996	98.933	98.810	98.774	98.878
	157	99.205	99.115	99.034	98.939	99.073
	B255	92.890	89.010	85.648	89.456	89.251
S5	0	0.222	0.356	0.233	0.415	0.307
	1	0.000	0.000	0.000	0.009	0.002
	2	0.189	0.144	0.141	0.189	0.166
	3	0.072	0.045	0.064	0.028	0.052
	4	0.026	0.083	0.064	0.113	0.072
	5	0.157	0.235	0.162	0.283	0.209
	6	0.091	0.144	0.141	0.217	0.148
	7	99.243	98.991	99.196	98.745	99.044
	157	99.400	99.227	99.358	99.038	99.255
	B255	92.820	88.693	87.609	92.604	90.432

† All event grades except B255 are ASCA grades. Here B255 stands for ACIS bit grade code 255 (i.e., all pixels above threshold).

Table 1.73: Fraction of Background Events per Event Grade Measured at XRCF in the Passband 0.1–10 keV for Detectors S0, S2, S4, and S5

Flight Device	Event[†] Grades	Fraction of Events per Event Grade				
		Quad A	Quad B	Quad C	Quad D	Mean
		(%)				
S1*	...	...	...	...	...	...
S3	0	5.667	5.579	5.148	5.678	5.518
	1	0.000	0.070	0.071	0.000	0.035
	2	8.000	9.275	9.944	8.754	8.993
	3	2.917	3.138	2.186	2.839	2.770
	4	2.250	2.650	2.680	2.050	2.408
	5	5.250	4.393	4.443	5.836	4.981
	6	14.250	11.018	13.329	12.145	12.685
	7	61.667	63.877	62.200	62.697	62.610
	157	66.917	68.340	66.714	68.533	67.626
	B255	4.333	3.835	4.020	4.180	4.092

[†] All event grades except B255 are ASCA grades. Here B255 stands for ACIS bit grade code 255 (i.e., all pixels above threshold).
* See note for detector S1 in Table 1.70.

Table 1.74: Fraction of Background Events per Event Grade Measured at XRCF in the Passband 0.1–10 keV for Detectors S1 and S3